JOINT INSTITUTE FOR NUCLEAR RESEARCH
Frank Laboratory of Neutron Physics

FINAL REPORT ON THE
SUMMER STUDENT PROGRAM

Structure investigations of biogenic ferrihydrite samples by small-angle scattering of neutrons and X-rays

Supervisor:
Dr. Maria Balasoiu

Student:
Ekaterina Pakhomova,
Russia, Dubna State University

Participation period:
August 01 – August 31

Dubna, 2016

Ferrihydrite, an iron oxide hydroxide, is a much widespread material [1–9]. It enters, as a constituent, in various bands of environments, such as clays and soils, soluble fraction of weathered rocks, ground and hydrothermal spring waters, etc. Of all the types of iron oxides, ferrihydrite has a largest distribution in living organisms, where it is found in the form of ferritin, an iron storage protein. Moreover, ferrihydrite is found to be present in some microbial communities, where it is produced by bacteria as a result of their metabolism [1–4]. In addition to this, ferrihydrite has been found in several extraterrestrial materials, as meteorites and interplanetary dust particles [1].

Ferrihydrite, being an antiferromagnetic oxyhydroxide in the bulk, in nanophase state yields the particles which possess permanent magnetic moments. The latter originate from the loss of compensation in a finite spin assembly of a particle where the number of surface spins is by no means negligible in comparison with that in the bulk. The two most known forms of these magnetic ferrihydrite particles are distinguished with respect to the number of lines in their respective X-ray diffraction patterns [5–7]. Accordingly varies the nanocrystal size: from 2– 4 nm in 2-line modification to 5–6 nm in 6-line modification. The 6-line ferrihydrite was identified as a mineral by International Mineralogical Association (IMA) in 1973 [8,9]. The less crystalline 2-line ferrihydrite, on the other hand, is not believed to be a mineral. In comparison with most minerals, both 2-line and 6-line ferrihydrites show very broad diffraction lines that makes it difficult to extract accurate structural information. With its high specific surface area [10], ferrihydrite is a very reactive substance. It can interact, either by surface adsorption or by co-precipitation, with a number of environmentally important chemical species, including arsenic, heavy metals e.g. lead or mercury, with phosphates and many organic molecules.[1]

Many microorganisms are known to produce inorganic nanostructures and nanoparticles with properties similar to chemically synthesized materials, while exercising strict control over size, shape and composition of the particles. Examples include the formation of magnetic nanoparticles by magnetostatic bacteria, the production of silver particles by *Pseudomonas stutzeri*, synthesis of nanoscale, semiconducting CdS crystals in the yeast *Schizosaccharomyces pombe*, and the formation of palladium nanoparticles using sulphate reducing bacteria in the presence of an exogenous electron donor [1-7]. The ability of bacteria, fungi, actinomycetes, yeast, algae and plants to accumulate gold ions from solution has been reported and the synthesis of gold nanoparticles has been successfully demonstrated in a range of organisms including *Bacillus sp.*, fungal species such as *Verticillium* and *Fusarium*, actinomycete such as *Rhodococcus* and *Thermomonospora* and lactic acid bacteria [1-11].The interest also extends to the synthesis of nanostructures such as nanowires and the assembly of nanoparticles using biological templates such as S-layers and viruses [12, 13], DNA, proteins [14, 15]

In the present work samples containing biogenic ferrihydrite nanoparticles produced by bacteria Klebsiella oxytoca are investigated. We note that biogenic minerals often turn out to be in fact composites where nano- or micro-scale amorphous or crystalline materials are densely mixed with organic molecules. Due to that, complex hierarchical structures from nanometer to the macroscopic scale are formed. The mechanisms of biomineral formation are not fully understood, and while they are of interest in their own right yielding new insights into the genetic control of biological structure [15], they may also provide new concepts for artificial structures and inspire solutions in design and engineering of nanoscale materials.

To study the structure of the colloidal systems, scattering techniques are certainly the more appropriate tool. The microscopic observation is normally difficult and, moreover, experiments performed in reciprocal space average over very large volumes and ignore defects and irrelevant details which can dominate in the real space image.[16]

Because of characteristic sizes in colloidal systems, light, X rays and neutrons are more using probes in it. In the case of light and X rays, the interaction is between electric fields of the radiation and the electronic charges. The main difference between these two technologies is their wavelength. Neutrons because they have no electric charge, interact in all situations with the nuclei exclusively. Comparing with the size present in colloidal systems, one can deduce that neutrons are very often the more appropriate way for the study of the structure, most of the time at small scattering angles, close to the beam transmitters through the sample without interaction. This constitutes the technique of small angle neutron scattering or SANS.[17]

The investigations were carried out in Frank Laboratory of Neutron Physics (FLNP), JINR, Dubna, at the IBR-2 reactor on the YuMO instrument. The layout of the YuMO instrument is presented in Fig.1 and the main its parameters are in the Table 1.

YuMO

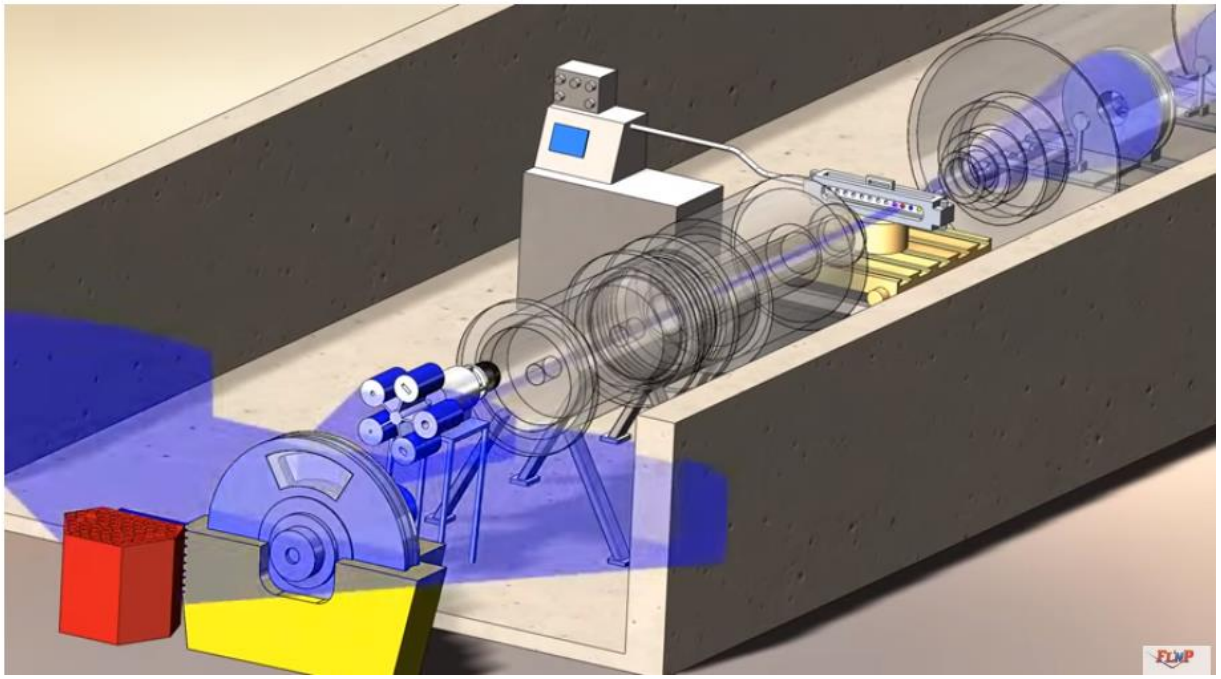

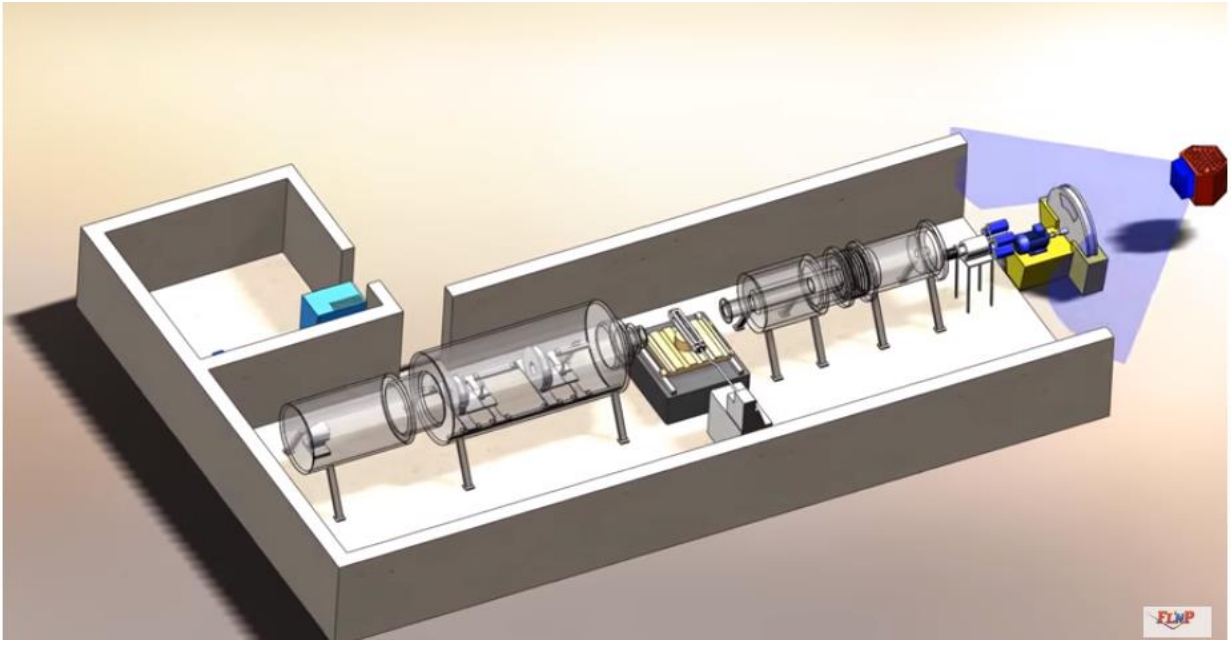

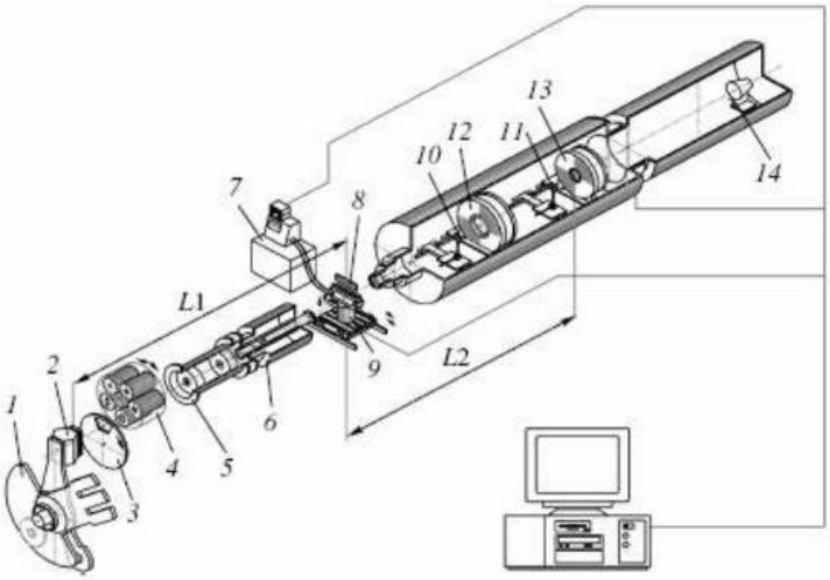

Figure 1. YuMO SANS TOF spectrometer in function at IBR-2 reactor [1, 2, 3]: 1) movable reflector; 2) moderator/cold moderator; 3) chopper; 4) first collimator; 5) vacuum tube; 6) second collimator; 7) liquid bath thermostat; 8, 9) place for the electromagnet during SANS experiments on magnetic samples; 10, 11) V, graphite, H 2 O standards; 12) circular detector of thermal neutrons; 13) PSD circular detector of thermal neutrons; 14) detector of direct beam.

Fig.1 YuMO instrument

Information could be obtained by SANS includes sizes, spatial correlations and shapes of particles, agglomerates, pores and fractals in crystalline and in amorphous states as well as in solution on a length scale ranging from 1 nm up to several hundred nanometers. Also: phase transitions, degree of polydispersity, aggregation numbers, molecular weight and geometric peculiarities.

Special methods are subdivided into two groups: contrast variation method and label method. The contrast variation method includes determination of object density and investigation of system homogeneity. The label method includes analysis of density distribution in studied object.

Main parameters of YuMO instrument **Table 1**

Parameters	Value
Flux on the sample (thermal neutrons)	10^7– $4x10^7$ n/(s cm^2)
Used wavelength	0.5 Å to 8 Å
Q-range	$7x10^{-3}$ – 0.5 $Å^{-1}$
Dynamic Q-range	q_{max}/q_{min} up to 100
Specific features	Two detectors system, central hole detectors
Size range of object *	500 – 10 Å
Intensity (absolute units -minimal levels)	0.01 cm^{-1}
Calibration standard	Vanadium during the experiment
Size of beam on the sample	8 – 22 mm^2
Collimation system	Axial
Detectors	He^3 -fulfiled, home made preparation, 8 independent wires
Detector (direct beam)	^{6}Li-convertor (home made preparation)
Condition of sample	In special box in air
Q-resolution	low, 5-20%
Temperature range	-50°C -+130°C (Lauda)
Temperature range	700 C (Evrotherm)
Number of computer controlled samples	14
Background level	0.03 – 0.2 cm^{-1}
Mean time of measurements for one sample	1 h +
Frequency of pulse repetition	5 Hz

Electronic system	VME
The instrument control software complex	SONIX
Controlling parameters	Starts (time of experiments), power, vandium standard position , samples position, samples box temperature, vacuum in detectors tube.
Data treatment	SAS, Fitter

Improvement of the YuMO instrument was going in accordance with the developed and submitted for the consideration project and plan. Main goals of this work are increasing of q-range, shortening of data acquisition time and optimisation of the instrument to new conditions. The changes are concerned almost all basic elements of the YuMO: detector, data acquisition, collimation systems as well as sample environment conditions.

The main inconvenient of neutron scattering is the weak intensity of the available neutron sources and their rarity. In spite of complex techniques, that allow the detection of magnitude of the minimum of scattered intensity that can be detected in a reasonable time. Other inconvenient of neutron scattering, when used for the study of structures, come from their low energy and from the different ways they can couple with a nucleus.[18-20]

The principle of all coherent scattering process is the interference of the waves scattered by individual centers: the nuclei in the case of neutrons, the electrons in the case of electromagnetic waves (light, X rays).

Neutrons are scattered by nuclei. The scattering due to an isolated nucleus is isotropic.

The total scattered intensity by an ensemble of N nuclei occupying a volume V_0 includes all the possible N^2 interferences and can be written:

$$I(Q) = \frac{1}{V_0} < |\sum_{i=1}^{N} b_i \, exp(iQ.r)\,|^2 >= \frac{1}{V_0} < \sum_{i,j} b_i b_j \, exp\left|iQ.(r_i - r_j)\right| >$$

where b_i is the coherent scattering length of nucleus *I* and wave vector *Q* is with the magnitude $Q = 4\pi\sin(\theta/2)/\lambda$.

In a SANS experiment, the conditions are generally chosen in such a way that Q^{-1} is larger than the interatomic distances in condensed matter. As a consequence, the detailed description of the structure at the atomic level is not possible. SANS are used in situations where the important physical aspects (size, range, etc.) occur at distances extending typically from 10 to 1000 A.

Small-angle diffusion scattering is the representative method of structure analysis with low resolution. Expression for one macromolecule in solution (differential scattering section) can be received by averaging on orientations. For isotropic solutions averaging leads to result which is named as Debye's formula:

$$\langle\frac{d\sigma}{d\Omega}\rangle = \int_V \int_{V'} \rho(r)\rho(r')\frac{sinx|r-r'|}{x|r-r'|}\,dV\,dV' \qquad (1)$$

Intensity of scattered neutrons is even function of length of scattered vector κ that is natural to the isotropic diffuser.

Each macromolecule has the characteristic size *L*, from expression (1) at once some main properties of the law of dispersion follow. At - $xL \leq 1$ about multiplier of $sinxlx=1$, scattered intensity $\sim\rho^2V^2$ and not depends neither on internal structure, nor on macromolecule form. At $xL \approx 1$ intensity generally depends on the sizes and form of macromolecule. At $xL \geq 1$ in principle there is sensitivity to parts internal structure of macromolecule, but oscillating character integrand leads to fast attenuation of intensity with growth *x* (generally $\sim I/(xL)^4$). The main part of scattered intensity falls on the $xL \lesssim 1$ that at the typical sizes macromolecules to 50 A and wave length of neutron

5 A there corresponds $sin(\theta/2) \leq \lambda/4\pi L = 8\times10^{-3}$ or $\leq 1°$. The last circumstance explains origin of the term «small-angle scattering».[21, 23]

In 1939 Guinier has taken important step on the way of transformation of formula (1) in the working tool, having used decomposition of $sinx/x = 1 - x^2/3! + x^4/5! - \ldots$ and having held in it the first two members, formula (1) is possible to simplify further:

$$\left\langle \frac{d\sigma}{d\Omega} \right\rangle = \left(\int_V \rho(\mathbf{r})\, dV \right)^2 \left(1 - \frac{1}{3} \varkappa^2 \int_V \rho(\mathbf{r})\, r^2\, dV \Big/ \int_V \rho(\mathbf{r})\, dV + \ldots \right) = \left(\int_V \rho(\mathbf{r})\, dV \right)^2 (1 - \varkappa^2 R_g^2/3 + \ldots), \quad (2)$$

where the R_g^2 is about matches definition of square of gyration radius of body with density equal to scattered density. Guinier has assumed that the good approximation of expression in the last bracket (2) is function $F^2(x) = \exp\left(-\frac{x^2 R_g^2}{3}\right)$ (3),

the R_g^2 parameter in which is the gyration radius (Guinier's approximation). The last expression is basis for definition «observed» gyration radius from experimental data by creation of so-called Guinier-graph *lnI(x2)* and slope fixing of its line section:

$$R_g^2 = -\frac{1}{3} d \ln I(\varkappa^2)/d\varkappa^2. \quad (3)$$

For homogeneous bodies of simple form *R* it is easy to calculate:

$R_{g0}^2 = \frac{3R_0^2}{5}$ - sphere with radius R_0

$R_{g0}^2 = (a^2 + b^2 + c^2)/5$ - three-axis ellipsoid with half shafts a, b, c

$R_{go}=L^2/12$ - infinitely thin rod of length of *L*

Rgo =$\overline{h_2}$ /6 - Gaussian ball with the mean square in distance between the ends of $\overline{h_2}$ [2-4]

Guinier's approximation is exact at $x^2 \to 0$ and is usually suitable in practice in area $x^2 R_g^2 < 1$. Deviations *I(x)* from approximation Guinier outside the Guinier's zone are served as the instruction on character of anisotropy (non- sphericity measure) of particle.

To find the full scattering length and gyration radius, first of all it is required to consider behavior of *I(Q)* in the field of the smallest scattering angles. Using *sinQr/Qr* function decomposition in a row of Macloren it is easy to show that Guinier's formula for initial part of scattered curve looks as follows $I(Q)=I(0)\exp(-Q^2R_g^2/3)$. To determine gyration radius by Guinier's method it's enough to take only beginning of the scattered curve.[22, 23]

The size of the most known small-angle parameter, particle gyration radius R_g, can be determined from slope of line section of dependence *lnI(Q)* from Q^2 (Guinier's approximation) that is easily proved by formula:

$$ln\, I(Q) \approx lnI(0) - Q^2 R_g^2/3 \qquad (4)$$

If the shape and dimensions of the particle are known, the evaluation of *I*(Q) is simple.

Normally, for a given shape, one evaluates the preceding integral for some arbitrary orientation of the particle relative to the Q vector, and then averages over all the possible orientations.[21]

The asymptotic behavior of *I*(Q) is general and independent of the shape of the particle. This is because at small Q, the spatial resolution is not sufficient to determine the shape, and only information about the size can be obtained. Under these conditions, *I*(*Q*) is given by the Guinier relation:

$$I(Q) = K^2 V^2 \exp\left(-\frac{Q^2 R_g^2}{3}\right) \qquad (5)$$

for $QR_g<1$ where R_g is the radius of gyration of the particle and V its volume. Data analysis in this regime is particularly reliable because the evaluation of R_g can be done with $I(Q)$ in arbitrary units.

At the other extreme, i.e. for values of Q much larger than the inverse of the smallest dimensions of the particle, the spatial resolution is too good and one observes only the interface between the particle and the solvent. However, in this regime, the Q dependence of I(Q) may be a function of the scale at which the surface is observed. Bale and Schmidt showed that, for a fractal surface of dimension D_s $(2\leq D_s<3)$, $I(Q)=AQ^{-(6-Ds)}$, with A given by $A=\pi N_0 K^2 \Gamma(5-D_s)\sin[\pi(D_s-1)/2]$ where N_0 is measure of the surface area.

In the ideal case where the interfacial region is sharp, one obtains the equation of Porod:

$I(Q)=2\pi K^2(S/V)Q^{-4}$ where S/V is the total area of the interface per unit of volume of the particle.[24]

Experimental SANS curves in the linear scale from studied sample is presented at Fig.2. The measured SANS spectra demonstrate quite smooth patterns over the whole available Q-range which points to high polydispersion of the studied system.

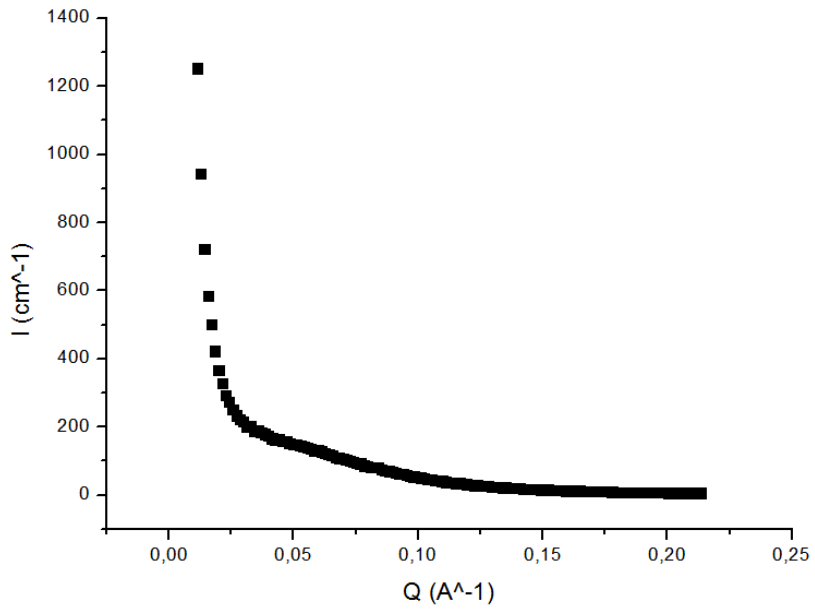

Fig.2 Experimental SANS curve in the linear scale

The experimental SANS curve in logarithmic coordinates are presented in Fig.3.

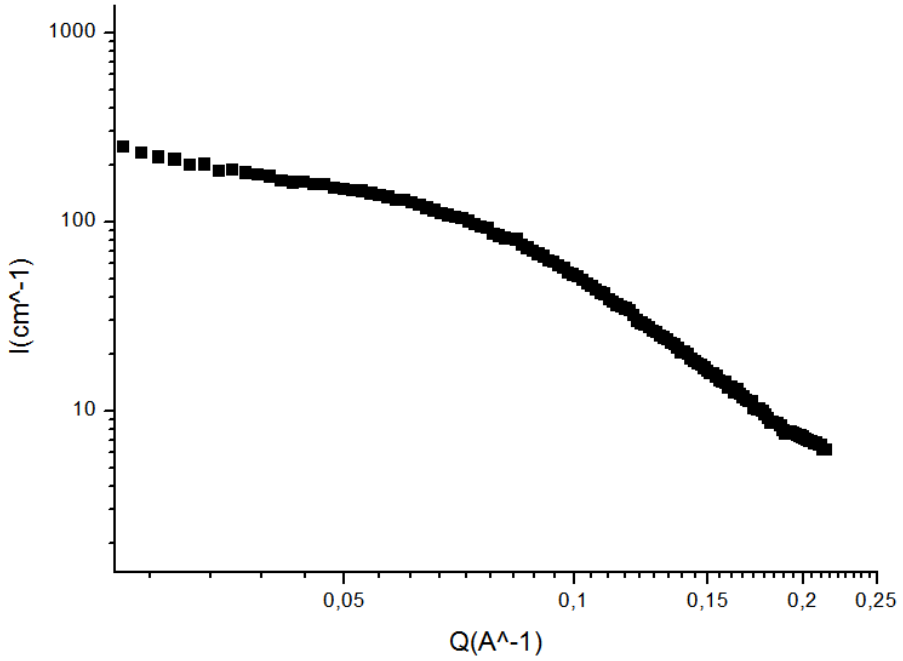

Fig.3 Experimental SANS curve in the logarithmic scale

Usually SANS curves are characterized by two main features: the Guinier region and the Porod region. Standard linear functions are applied within these regions to fit SANS data. The Guinier linear plot gives a value of a gyration radius that characterizes the size of the scattering particles. Therefore, from estimated fractal dimension the particle shape can be determined.

Further (Fig.4) in the field of very small angles to which it is possible to apply decomposition in Taylor expansion, it is possible to see that dependence has linear character. It is easy to show it from the formula $ln\, I(Q) \approx lnI(0) - Q^2R_g^2/3$, which turns out by logarithming of a formula $I(Q)=I(0)exp(-Q^2R_g^2/3)$.[23]

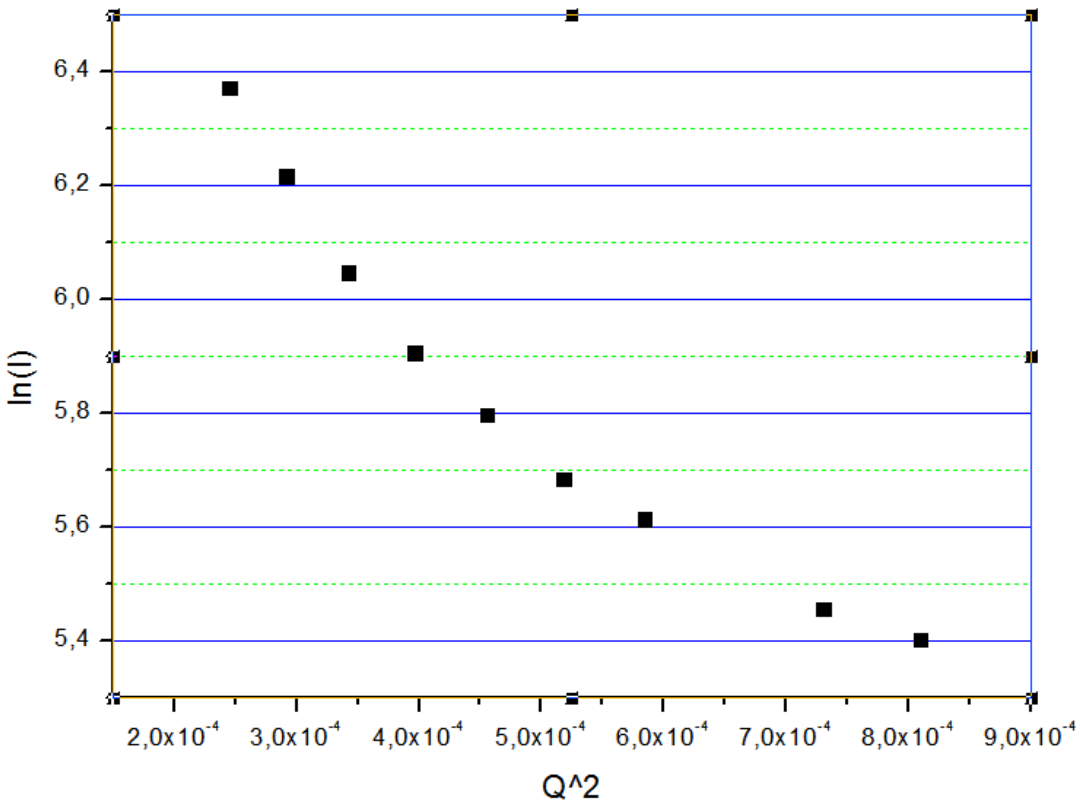

Fig.4 Experimental SANS curve in the region of the very small angles

The result of Guinier's approximation is presented in the Fig.5.

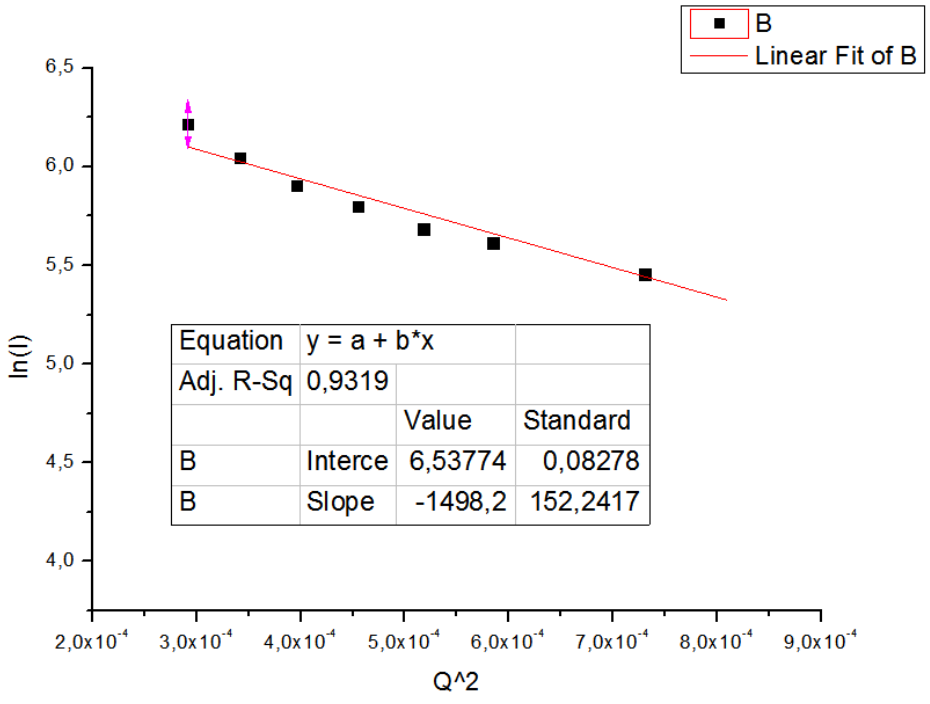

Fig.5 Guinier's approximation for SANS curve

Because $b=-1498\pm152$ and because of $b=-\frac{R_g^2}{3}$, the gyration radius is equal $R_g=67A$. The coefficient of determination is equal $R^2=0,94$. This confirms the high quality of the linear fit.

It should be noted that ferrohydrite particles often have different shapes that shows the SEM (scanning electron microscopy). The results of SEM are demonstrated in Fig.6.[2]

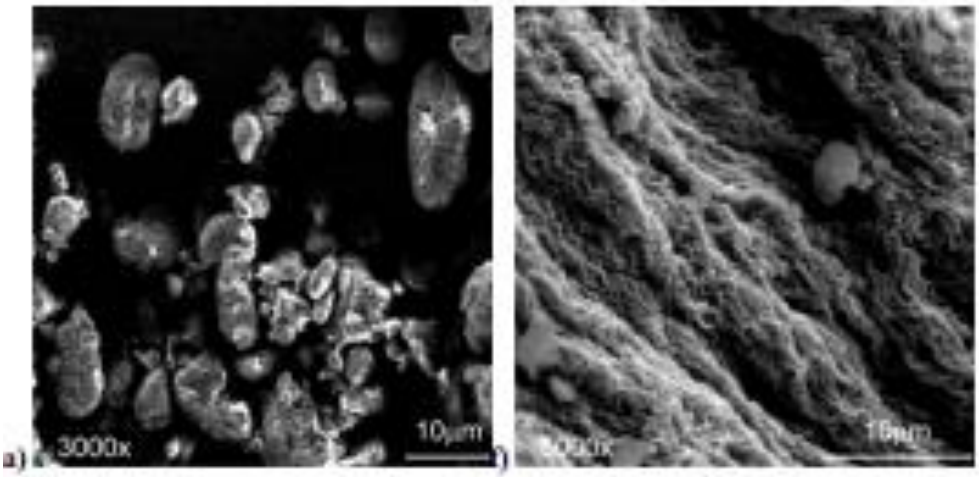

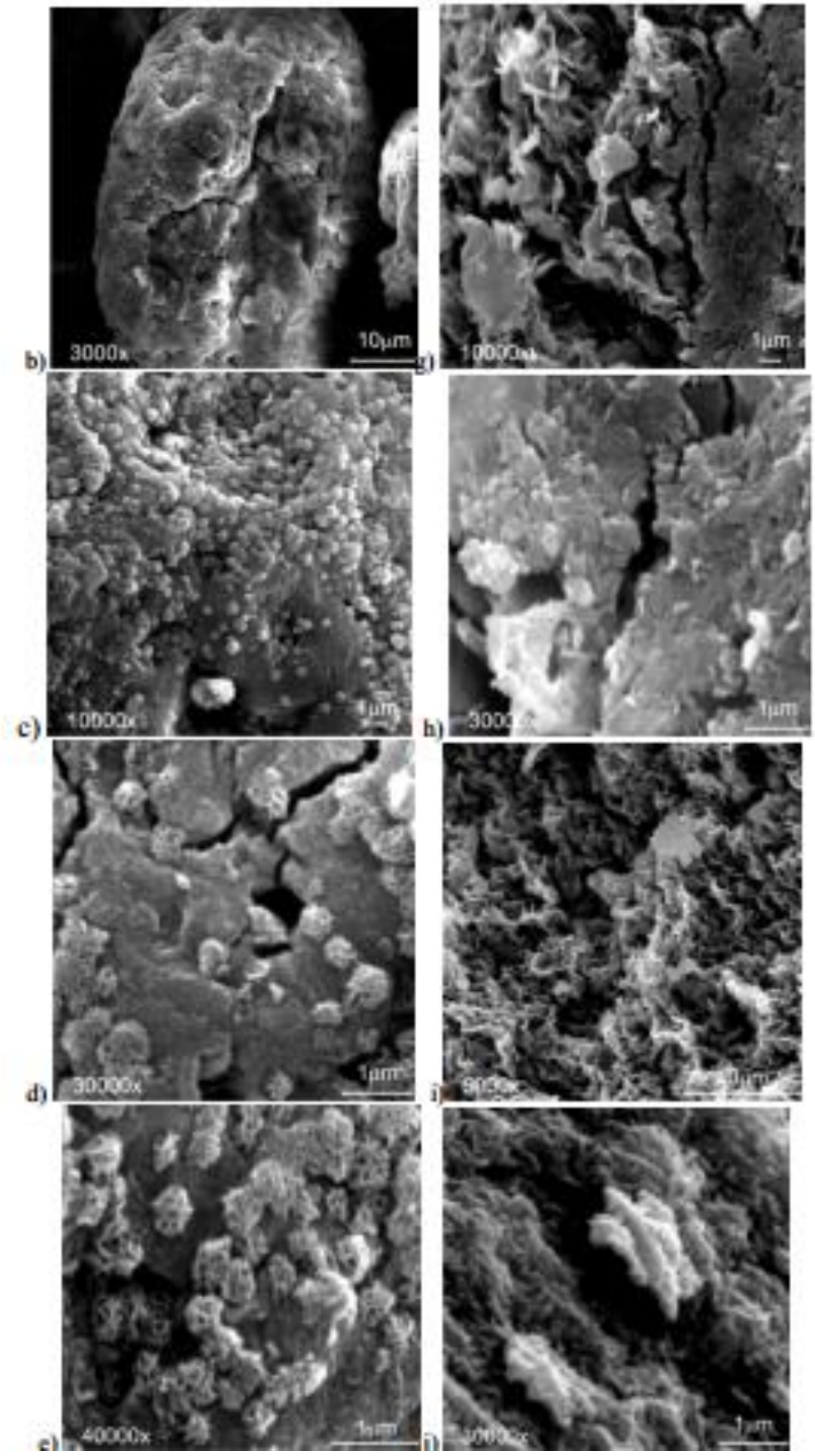

Fig.6 The SEM results for two samples containing ferrihydrite nanoparticles obtained by means of two different methods

The final conclusions: the SANS method has been studied, and also the investigation of biogenic ferrihydrite samples are carried out by SANS at the YuMO instrument. The gyration radius of scattered particles is determined in the field of very small angles by means of Guinier's approximation. It should be noted that as possible development of research can be the determination of the geometric characteristics of the scattered particles in the presence of SEM data.

[1] HIERARCHICAL STRUCTURE INVESTIGATIONS OF BIOGENIC FERRIHYDRITE SAMPLES

M. Balasoiu1, S.V. Stolyar, R.S. Iskhakov, L.A. Ishchenko, Yu.L. Raikher, A.I. Kuklin, O.L. Orelovich4, Yu.S. Kovalev, T.S. Kurkin, G.M. Arzumanian

[2] Structural investigation of biogenic ferrihydrite nanoparticles dispersion *M. BALASOIUa,e,*, L. A. ISCHENKOb, S. V. STOLYARb,f, R. S. ISKHAKOVb,f, Y. L. RAIKHERc, A. I. KUKLINa, D. V. SOLOVIOVa, T. S. KURKINd, D. ARANGHELe, G. M. ARZUMANIANa aJoint Institute of Nuclear Research, Dubna, 141980, Russia bSiberian Federal University, 660041, Krasnoyarsk, Russia cInstitute of Continuum Media Mechanics, Ural Branch of RAS, 614013, Perm, Russia dInstitute of Synthetic Polymer Materials RAS, Moscow, 117393, Russia eNational Institute of Physics and Nuclear Engineering, P.O.BOX MG-6, Bucharest, Romania fInstitute of Physics, Siberian Branch of RAS, 660036, Krasnoyarsk, Russia*

[3] M. Sastry, A. Ahmad, M. I. Khan, R. Kumar, Current Science *85*(2), 162 (2003).

[4] C. Lang, D. Schuler, J. Phys.: Condens. Mat. *18*, S2815 (2006).

[5] D. Mandal, M. E. Bolander, D. Mukhopadhyay, G. Sarkar, P. Mukherjee, Appl. Microbiol. Biotechnol. *69*, 485 (2006).

[6] M. Gericke, A. Pinches, Hydrometallurgy *83*, 132 (2006).

[7] P. Mohanpuria, N. K. Rana, S. Kumar Yadav, J. Nanopart. Res. *10*, 507 (2008).

[8] N. Krumov, I. Perner-Nochta, St. Oder, V. Gotcheva, A. Angelov, C. Posten, Chem. Eng. Technol. *32*, 1026 (2009).

[9] K. B. Narayanan, N. Sakthivel, Adv. in Colloid and

Interface Science *156*(1-2), 1 (2010).

[10] Ref. of [4].

[11] Ref. of [5].

[12] Ref. of [6].

[13] Ref. of [7].

[14] M. Sara, U. B. Sleytr, J Bacteriol. *182*, 859 (2000).

[15] B. Schuster, P. C. Gufler, D. Pum, et al., IEEE TransNanobioscience *3*(1), 16 (2004).

[16] K. K. W. Wong, S. Mann, Adv. Mater. *8*, 928 (1996).

[17] J. Yang, J.Y. Lee, H. Too, G. M. Chow, L. M. Gan,Chemical Physics *323*, 304 (2006).

[18] A. Bharde, D. Rautaray, V. Bansal, A. Ahmad,I. Sarkar, S. M. Yusuf, M. Sanyal, M. Sastry, Small

[19] Guinier, A. and Fournet, G., Small-Angle Scattering of X-Rays // John Wiley & Sons Inc., New York 1955.

[20] Glatter, O. and Kratky, O., Small-Angle X-Ray Scattering//Academic Press, London, 1982.

[21] Feigin, L. A., and D. I. Svergun. 1987. Structure Analysis by Small-Angle. X-Ray and Neutron Scattering. New York: Plenum Press. pp 33, 1988. Бекренев А.Н., Миркин Л.И. Малоугловая рентгенография деформации и разрушения материалов // М.: Изд-во МГУ, 1991. - 246 с.

[22] Higgins Julia S. and Benoit C. Polymers and Neutron Scattering// Clarendon press, Oxford, 1994.

[23] Ю.М.Останевич, И.Н.Сердюк. Нейтронографические исследования структуры биологических макромолекул. Успехи физических наук, том 137, вып.1, 1982 г.

[24] International Conference on Small-Angle Scattering, Journal of Applied Crystallography, Vol.21. Part 6. December 1988 (pp.581-1009).